The International Journal of Advanced Manufacturing Technology (2021) 115:3679–3687
https://doi.org/10.1007/s00170-021-07426-3

ORIGINAL ARTICLE

# Double-sided self-pierce riveting of dissimilar materials

Luis M. Alves[1] · Rafael M. Afonso[1] · Patric T. Pereira[1] · Paulo A. F. Martins[1]

Received: 30 March 2021 / Accepted: 3 June 2021 / Published online: 9 June 2021


## Abstract

This paper is focused on double-sided self-pierce riveting (DSSPR) of overlapped sheets made from dissimilar materials with very different mechanical strengths. The methodology draws from previous work on sheets made from similar or identical materials and the extension to dissimilar materials is built-upon a combined experimental and numerical investigation that makes use of AA5754-H111 aluminum and polyvinylchloride sheets. Results show that reengineering of conventional DSSPR by modification of the chamfered rivet angles to account for the different resistances to penetration of the two materials is not effective, because it cannot solve the formation of asymmetric mechanical interlockings with very small undercuts in the harder sheet material. The proposal of an innovative two-stroke DSSPR process in which the tubular rivet is first forced through the harder sheet with the help of a dedicated compression tool, and only subsequently pressed through the softer sheet, proves to be effective in obtaining symmetric joints with good undercuts in both sheets. Destructive shear tests confirm the good performance of the joints produced by means of the new proposed two-stroke DSSPR.

**Keywords** Joining by forming · Double-sided self-pierce riveting · Dissimilar materials · Experimentation · Finite element method

## 1 Introduction

Self-pierce riveting (SPR) is an increasingly used joining by forming process to attach two or more overlapped sheets (Fig. 1a). The process is carried out in a single stroke during which a semi-tubular rivet is pierced through the sheets, without perforating the lower sheet. Progressively flaring of the rivet ends during piercing ensures the creation of a mechanical interlocking based on a radial undercut, as it is shown in Fig. 1b.

SPR is employed in a wide range of industrial applications with special emphasizes on the assembly of automotive components [1], as a result of three fundamental advantages over alternative joining processes: (i) the elimination of the need to pre-drill holes in the sheets, which is required by mechanical fastening; (ii) the avoidance of curing time and surface preparation of sheets, which is mandatory for adhesive bonding; and (iii) the removal of the heat-cooling cycles of welding that gives rise to distortions, damage in pre-coated sheets, and modifications in the microstructure of the materials.

The deformation mechanics of SPR [2, 3], its failure mechanisms [4] and applications have been analyzed and discussed by several researchers and the main results and conclusions obtained from these investigations are summarized in two recent state-of-the-art review papers [5, 6].

Through the reading of these and other articles in the field, the main drawbacks in the application of SPR can be identified as (i) the limited range of the total sheet thicknesses (between 1.5 and 4 mm), (ii) the necessity of placing the thinner or softer sheets on the rivet side, and (iii) the formation of material protrusions above and below the sheet surfaces.

This means that the high flexibility, environmental friendliness, and room temperature operation advantages of SPR can be outweighed by the disadvantages arising from the difficulties in joining thick sheets made from dissimilar materials with local geometry changes caused by the mechanical interlockings.

✉ Paulo A. F. Martins
pmartins@tecnico.ulisboa.pt

Luis M. Alves
luisalves@tecnico.ulisboa.pt

Rafael M. Afonso
rafael.afonso@tecnico.ulisboa.pt

Patric T. Pereira
patric.pereira@tecnico.ulisboa.pt

[1] IDMEC, Instituto Superior Técnico, Universidade de Lisboa, Av. Rovisco Pais, 1049-001 Lisboa, Portugal

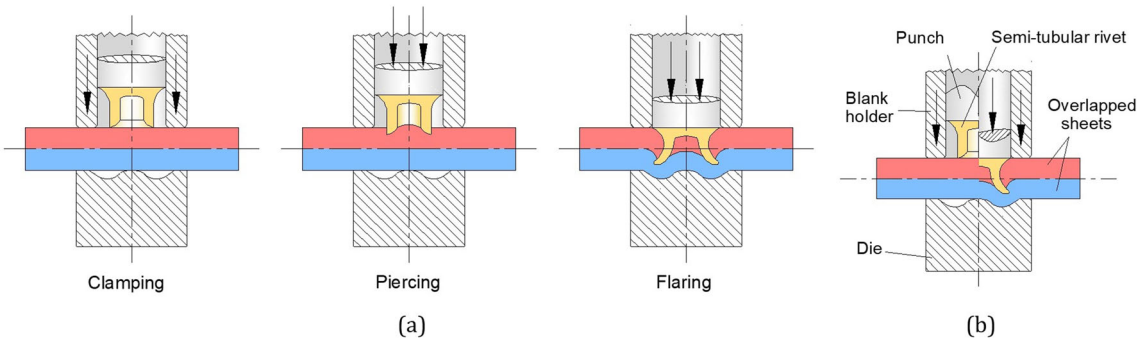


**Fig. 1** **a** Different stages in self-pierce riveting of two overlapped sheets with (**b**) main notation

The first step to address and solve some of the abovementioned drawbacks was done by Kato et al. [7], who introduced a new joining by forming process capable of producing invisible mechanical interlockings in overlapped sheets. The process is shown in Fig. 2 and consists of pressing a tubular rivet with chamfered ends into two adjoining sheets by compression. The formation of the undercut is ensured by flaring of the rivets ends during piercing like in SPR, and, according to the authors, the best performance in destructive tests is obtained for tubular rivets with chamfered angles $\alpha$ in the interval [45, 60] degrees.

Subsequent work on DSSPR by Huang et al. [8, 9] was focused on the final alignment between sheets and rivets with the aim of preventing the formation of asymmetric mechanical interlockings caused by incorrect positioning and/or initial obliquity of the rivets. They proposed a new rivet geometry with inner and outer flanges at the mid rivet height and confirmed its effectiveness in reducing the formation of asymmetric joints by means of experimental and numerical simulative tests carried out on AA6063 aluminum sheets and AISI 304 stainless steel rivets.

Alves et al. [10] performed experimental and finite element simulations on DSSPR with plain tubular rivets without flanges to characterize the deformation mechanics, determine its formability limits, and evaluate the performance of the resulting joints by means of pull-out and shear destructive tests. The work was performed in AA5754-H111 aluminum sheets and AISI 304 stainless steel tubular rivets with different chamfered angles and confirmed that best performances are obtained for rivets having chamfered angles $\alpha$ in the interval [45, 60] degrees. The work also showed that asymmetric deformation may be minimized (or, even prevented) by ensuring good positioning and geometric control of the tubular rivets.

In a recent work, Alves et al. [11] extended the application of DSSPR to polymer sheets through its application to the connection of polyvinylchloride sheets with AISI 304 stainless steel tubular rivets.

The results obtained in the abovementioned investigations allow concluding on the following main advantages of DSSPR against SPR: (i) the capability of joining thick sheets, because the process is independent from sheet thickness; (ii) the invisibility of the joints, because the mechanical interlockings are hidden inside the overlapped sheets; (iii) the absence of material protrusions; (iv) the avoidance of dedicated dies placed below the lower sheet; and (v) the simpler and easier to fabricate geometry of the rivets.

However, there is a fundamental question to be addressed with respect to the utilization of DSSPR that is often claimed to limit its overall applicability—the aptitude to connect sheets made from dissimilar materials with very different strengths.

Under these circumstances, this paper is focused on the application of DSSPR to the connection of sheets made of AA5754-H111 aluminum and polyvinylchloride (PVC) at ambient temperature. The work is supported by experimentation and finite element simulation and two main strategies are investigated. The first strategy analyzes the potential of extending the basic single-stroke working principle of DSSPR by modification of the chamfered angles $\alpha$ of the rivets to

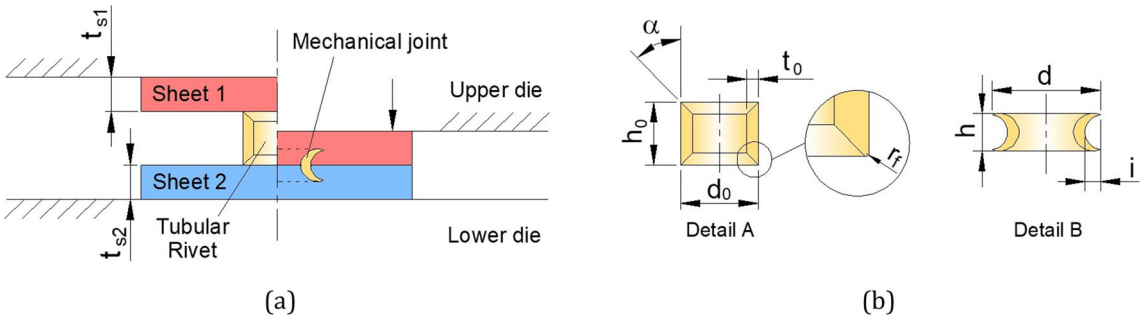


**Fig. 2** **a** Double-sided self-pierce riveting with (**b**) details of the tubular rivet before and after joining of the two sheets

account for the different resistances to penetration derived from the different strengths of the aluminum and PVC sheets. The second strategy introduces a new two-stroke DSSPR concept that circumvents the problems related to the formation of asymmetric mechanical interlockings in applications of single-stoke DSSPR and can produce good symmetric mechanical interlockings in joints made from dissimilar materials with very different strengths.

## 2 Methods and procedures

### 2.1 Mechanical characterization of the materials

The work was carried out in commercial AA5754-H111 aluminum and polyvinylchloride sheets with 5 mm thickness and AISI 304 stainless steel tubes with an outer diameter of 10 mm and a wall thickness of 1.5 mm. The stress-strain curves of the materials at ambient temperature were obtained by means of tensile and stack compression tests that were performed by the authors in previous investigations on DSSPR [10, 11]. The tests were done in a hydraulic testing machine (Instron SATEC 1200 kN) with a crosshead speed of 5 mm/min and the stress-strain curves are shown in Fig. 3. The elastic properties of the materials are provided in Table 1.

### 2.2 Experimental workplan

The main process parameters of DSSPR were previously identified by the authors [10, 11] as (i) the upper and lower sheet thicknesses $t_{si}$, and (ii) the outer diameter $d_0$, (iii) the height $h_0$, (iv) the wall thickness $t_0$, (v) the chamfered angle $\alpha$, and (vi) the fillet radius $r_f$ of the rivet ends (Fig. 2b). To prevent the experimental work from concentrating on subjects that were previously analyzed by the authors, it was decided to keep all but the chamfered angle $\alpha$ with constant values (Table 2) and to focus the attention on the influence of sheet materials with significant differences in strength, which were not considered earlier.

The objectives of the experimental workplan were accomplished by means of two different strategies. The first strategy, which coincided chronologically with the beginning of this investigation, aimed at extending the applicability of single-stroke DSSPR to dissimilar sheet materials with significant differences in strength.

The idea behind this first strategy was centered on the modification of the chamfered angle $\alpha$ of the rivet ends to find an appropriate combination of values that can modify the evolution of piercing and flaring in both sheets in such a way that symmetric mechanical interlockings are produced. The first set of test runs made use of rivets having equal chamfered angles $\alpha$ in the contact with the aluminum and PVC sheets ($\alpha_{alu} = \alpha_{PVC}$). The second set of test runs explored the possibility of using different chamfered angles ($\alpha_{alu} \neq \alpha_{PVC}$) in the contacts with the two different sheets.

The second strategy is based on a new two-stroke DSSPR concept in which the tubular rivet is first forced through the harder sheet with the help of a dedicated compression tool consisting of a bolster and a conical punch, and then pressed through the softer sheet to obtain a symmetric joint with good undercuts in both sheets. The working principle of the two-stroke DSSPR concept is shown in Fig. 4.

The experimental work plan also includes shear destructive tests to evaluate the differences in performance obtained from joints produced by single and two-stroke DSSPR.

### 2.3 Finite element modeling

The numerical simulation of single and two-stroke DSSPR was carried out with the in-house computer program i-form that is built upon the finite element flow formulation [12, 13]. The rivets and the sheets were assumed as deformable objects and the plastic deformation of the cross-sectional joints was assumed to be rotationally symmetric and limited to a region that includes the rivets and the neighboring sheet materials.

Figure 5 shows the initial and final meshes utilized in the finite element simulation of a cross-sectional joint produced by single-stroke DSSPR. The initial mesh was automatically generated and refined in the pre-processor module of i-form by combination of a grid-based and a quadtree subdivision strategy. The tools were modeled as rigid objects and discretized by means of linear contact-friction elements.

Friction was modeled according to the law of constant friction $\tau_f = mk$, where $m$ is the friction factor and $k$ is the flow shear strength. A friction factor $m$ equal to 0.1 was utilized on the contact interfaces between the deformable and rigid objects after checking the predicted forces that best matched the experimental results.

The computational time for a typical analysis using a convergence criterion for the velocity and residual equal to $10^{-3}$

**Table 1** Elastic properties of the materials utilized in this investigation

| Material | Yield stress (MPa) | Elasticity modulus (GPa) | Poisson ratio |
|---|---|---|---|
| AISI 304 | 205 | 193 | 0.29 |
| AA5754-H111 | 98.5 | 71.9 | 0.33 |
| PVC | 38 | 2.8 | 0.4 |

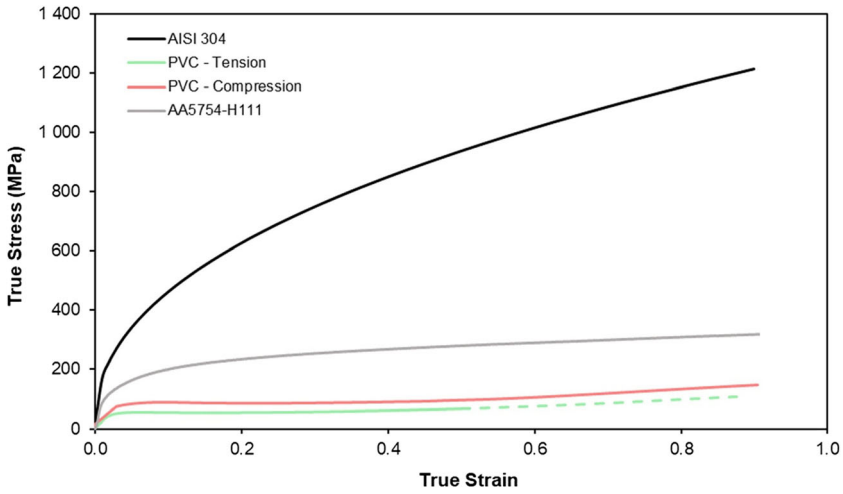


**Fig. 3** Stress-strain curves of the AA5754-H111 aluminum and PVC sheets and of the AISI 304 stainless-steel rivets

was approximately 15 min on a computer equipped with an Intel i7-5930K CPU processor.

## 3 Results and discussion

### 3.1 Conventional DSSPR

Figure 6 shows the experimental and finite element predicted cross-sections of three different test cases performed with conventional (single-stroke) DSSPR. The results included in the leftmost and central images of Fig. 6a and b were obtained from the first set of test runs and made use of rivets having equal chamfered angles ($\alpha_{alu} = \alpha_{PVC}$). The results included in the rightmost images of Fig. 6a and b were taken from the second set of tests that explored the utilization of different chamfered angles ($\alpha_{alu} = 30\,°$, $\alpha_{PVC} = 60°$).

As seen, the application of conventional single-stroke DSSPR to dissimilar materials with very different strengths works better when the chamfered angles of the tubular rivet ends are different to compensate for the greater or lesser penetration of the rivet into the sheets (refer to the rightmost pictures in Fig. 6a and b). In particular, the utilization of sharper chamfered angles $\alpha_{alu} = 30°$ at the rivet ends facing the aluminum sheets and blunter chamfered angles $\alpha_{PVC} = 60°$ at the opposite ends facing the PVC sheets ensures better mechanical interlockings in the aluminum sheets.

However, the results shown in Fig. 6 also reveal that the cross-sectional joints are asymmetric with the deformed rivets showing greater penetration in the PVC sheets than in the aluminum sheets due to greater mechanical strength of the latter. This horizontal asymmetry is often combined with signs of vertical asymmetry due to minor variations in the geometry of the rivets within the tolerances of fabrication.

Minor variations in the fillet radius $r_f$ and chamfered angles $\alpha$ of the tubular rivets are responsible for changes in piercing and progressive flaring of the rivet ends and, therefore, for differences in the final undercuts. In some cases, like that shown in the leftmost image of Fig. 6a, the combination of a sharp chamfered angle $\alpha = 30°$ with a fillet radius $r_f$ smaller than needed led to fracture because the tubular rivet ends started to behave as a cutting edge, whereas the corresponding numerical simulation performed with the nominal geometrical values does not predict fracture (leftmost image of Fig. 6b).

The conclusion from the attempt of extending the conventional single-stroke DSSPR to the connection of sheets with very different strengths is that although good mechanical interlockings can be achieved (e.g., center images of Fig. 6a and b), the observed horizontal and vertical asymmetries justify the need to develop a new process where these problems can be minimized or even eliminated. The results obtained with such a new process, designated as two-stroke DSSPR, will be analyzed in the following section of this paper.

However, before closing the discussion on the application of conventional single-stroke DSSPR to the connection of sheets made from dissimilar materials, there are two other subjects that worth being addressed: (i) the comparison

**Table 2** Process operating parameters that were utilized in the experimental tests performed with single and two-stroke double-sided self-pierce riveting (refer to Fig. 2 for nomenclature)

| **Rivet** | | | | |
|---|---|---|---|---|
| Material | $d_0$ (mm) | $h_0$ (mm) | $t_0$ (mm) | $\alpha$ (°) |
| AISI 304 | 10 | 8 | 1.5 | 30, 45, 60 |
| **Sheets** | | | | |
| Material | $t_{s1}$ (mm) | Material | $t_{s2}$(mm) | |
| AA5754-H111 | 5 | PVC | 5 | |

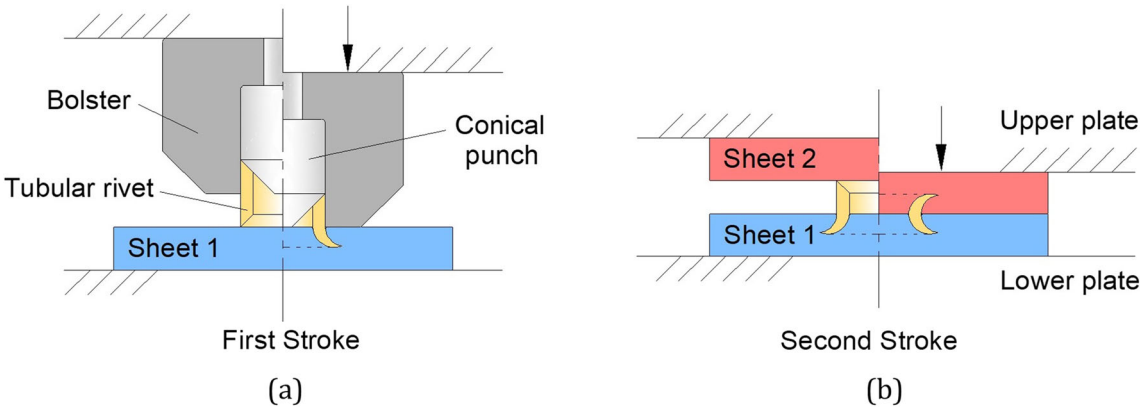


**Fig. 4** The new proposed two-stroke double-sided self-pierce riveting process at the (**a**) beginning and end of the first stroke and at the (**b**) beginning and end of the second stroke (i.e., end of the process)

between the experimental and finite element predicted geometries and (ii) the evolution of the riveting force with displacement during the punch stroke.

In fact, after halving the experimental specimens lengthwise to reveal its cross-sectional joints, there are material protrusions on the upper surface of the PVC sheets that are not visible in the finite element predicted geometries at the end of stroke. One can of course argue that the source of the mismatch is related to elastic recovery not being accounted in the finite element results shown in Fig. 6b, but the main reason for these differences is the excessive elastic recovery of the cross-sectional joints after halving the experimental test specimens lengthwise due to elimination of the circumferential constraint imposed by the plastically deformed material. This phenomenon cannot be simulated by finite elements and justifies the reason for the observed differences in the cross-sections. In fact, if elastic recovery after joining is considered, there is a predicted protrusion (Fig. 6c) considerably smaller than that shown in the experimental cross-section resulting from halving the specimen lengthwise (refer to the rightmost image in Fig. 6a).

Regarding the evolution of the riveting force with displacement, two main regions can be observed in Fig. 7. In region "A," the force increases progressively as the rivet is forced through the two sheets and the contact between the compression tool and the upper PVC sheet is limited to a zone placed above the rivet. Then, as the punch stroke approaches the end, the upper PVC sheet starts getting into full contact with the

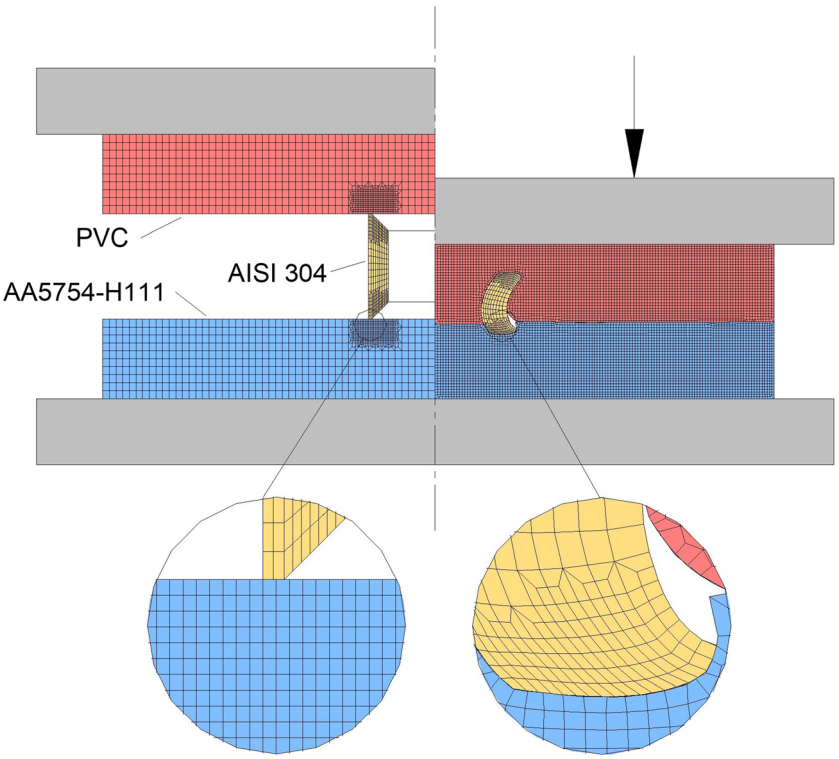


**Fig. 5** Finite element model utilized in the numerical simulation of the single-stroke double-sided self-pierce riveting of AA5754-H111 aluminum and PVC sheets with AISI 304 stainless-steel rivets at the beginning and end of the process ($\alpha_{alu} = 45°$, $\alpha_{pvc} = 45°$)

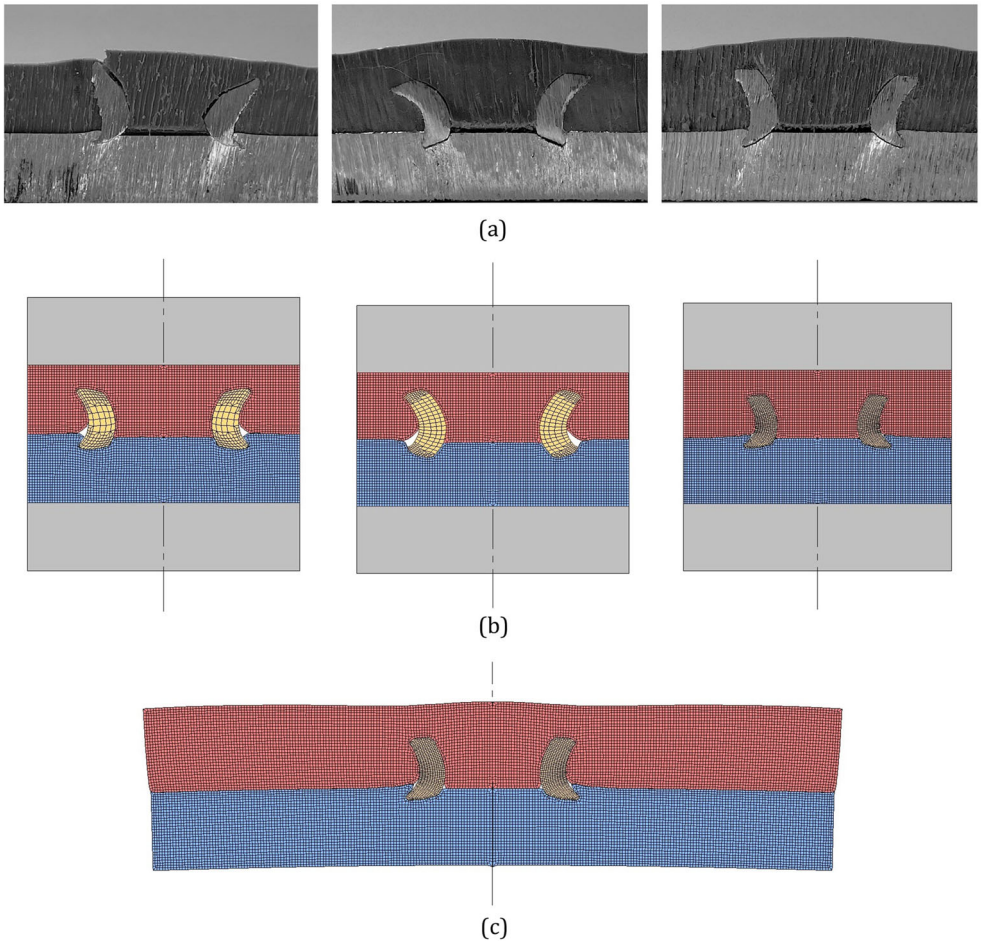


**Fig. 6** Single-stroke double-sided self-pierce riveting of AA5754-H111 aluminum and PVC sheets with AISI 304 stainless-steel rivets. **a** Experimental cross-sections for the test cases corresponding to values of the chamfered angles ($\alpha_{alu}$, $\alpha_{pvc}$) respectively equal to (left) (30°, 30°), (center) (60°, 60°), and (right) (30°, 60°). **b** Finite element predicted cross-sections for the test cases shown in **a**. **c** Elastic recovery after removing the test case shown in the rightmost image of **b** from tooling

upper compression die and the riveting force begins to grow steeply (refer to region "B"). The process must stop at the beginning of region "B" to avoid damaging the sheets and/or the tools.

The overall agreement between the experimental and the finite element predicted riveting forces is good and the fluctuations of the numerical estimates around the experimental values are attributed to the different remeshing operations that

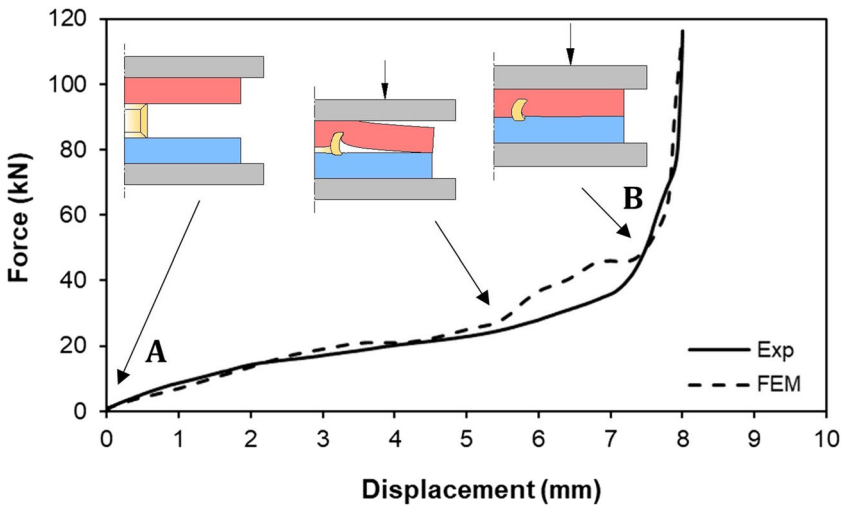


**Fig. 7** Experimental and finite element predicted evolution of the riveting force with displacement for the single-stroke double-sided self-pierce riveting of AA5754-H111 aluminum and PVC sheets with AISI 304 stainless-steel rivets ($\alpha_{alu} = 45°$, $\alpha_{pvc} = 45°$)

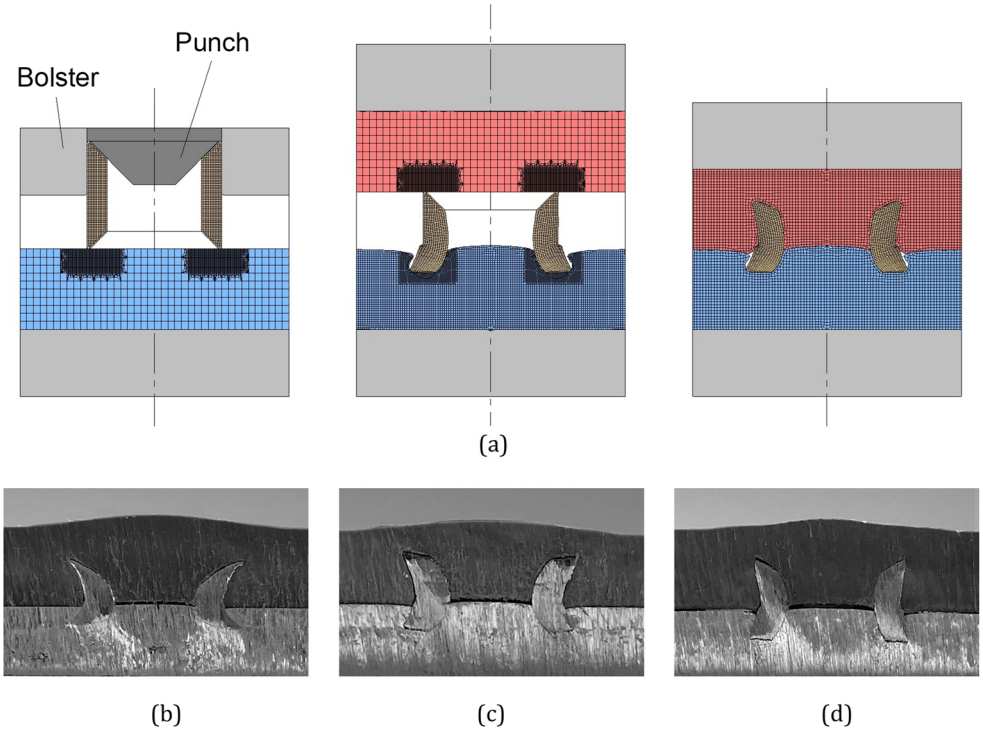


**Fig. 8** Double-stroke double-sided self-pierce riveting of AA5754-H111 aluminum and PVC sheets with AISI 304 stainless-steel rivets. **a** Finite element predicted evolution of the cross-sectional joint for the test case ($\alpha_{alu} = 45°$, $\alpha_{pvc} = 45°$). **b** Experimental cross-sections for the test case ($\alpha_{alu} = 30°$, $\alpha_{pvc} = 30°$).**c** Experimental cross-sections for the test case ($\alpha_{alu} = 45°$, $\alpha_{pvc} = 45°$).**d** Experimental cross-sections for the test case ($\alpha_{alu} = 60°$, $\alpha_{pvc} = 60°$)

were performed during the numerical simulation of the process.

### 3.2 Two-stroke DSSPR

Figure 8a presents the finite element simulation of the experimental test case ($\alpha_{alu} = 45°$, $\alpha_{pvc} = 45°$) shown in Fig. 8c to provide a deeper insight and a better understanding of the working principle of the two-stroke DSSPR. As seen in Fig. 8a, the tubular rivet is firstly forced through the aluminum sheet by means of a dedicated compression tool consisting of a bolster and a conical punch to create a mechanical interlocking between the lower rivet end and the aluminum sheet. Subsequently, the compression tool is removed to allow the PVC sheet to be placed over the rivet and compressed to obtain the missing interlocking at the opposite end of the tubular rivet.

As seen from the finite element simulation results and from the photographs of the cross-sectional joints that are included in Fig. 8b–d, the new two-stroke DSSPR is effective in minimizing both the horizontal and vertical asymmetries. The improvement in horizontal symmetry is due to a better control of the total amount of rivet height that is forced through the aluminum sheet during the first punch stroke. The lower sensitivity to variations in manufacturing tolerances, which are responsible for the vertical asymmetries that were observed in the single-stroke DSSPR, is because rivets are now guided during piercing and flaring in the sheet with greater mechanical strength.

The best mechanical interlockings were found for chamfered angles ($\alpha_{alu} = \alpha_{pvc}$) with values in-between [30, 45] degrees (Fig. 8b and c). Values of undercut approximately equal to 0.92 mm were measured for the test case produced with rivets having chamfered angles ($\alpha_{alu} = 45°$, $\alpha_{pvc} = 45°$).

The evolution of the riveting force with displacement for the test case shown in Fig. 8a and c ($\alpha_{alu} = 45°$, $\alpha_{pvc} = 45°$) is given in Fig. 9. Two sets of curves are provided; the black curves starting in "I" are the experimental and finite element predicted evolutions for the first punch stroke whereas the gray curves starting in "II" and ending in "III" are for the second punch stroke.

As expected, the riveting forces during piercing and flaring of the tubular rivet in the aluminum sheet are higher than those in the PVC sheet. The total amount of displacement in the first and second punch strokes are also slightly different because the joint is not horizontally symmetrical—more rivet material was forced through the PVC sheet.

Still, one may conclude that the required maximum force is in the range of 100 kN, as in the case of conventional single-stroke DSSPR (refer to Fig. 7).

### 3.3 Destructive testing

In their previous investigations on conventional DSSPR of polymer [11] and metal sheets [10], authors concluded that the shear destructive forces are 6 to 10 times higher than the maximum peel forces. Because the low mechanical strength of PVC will continue to facilitate the extraction of the stainless-

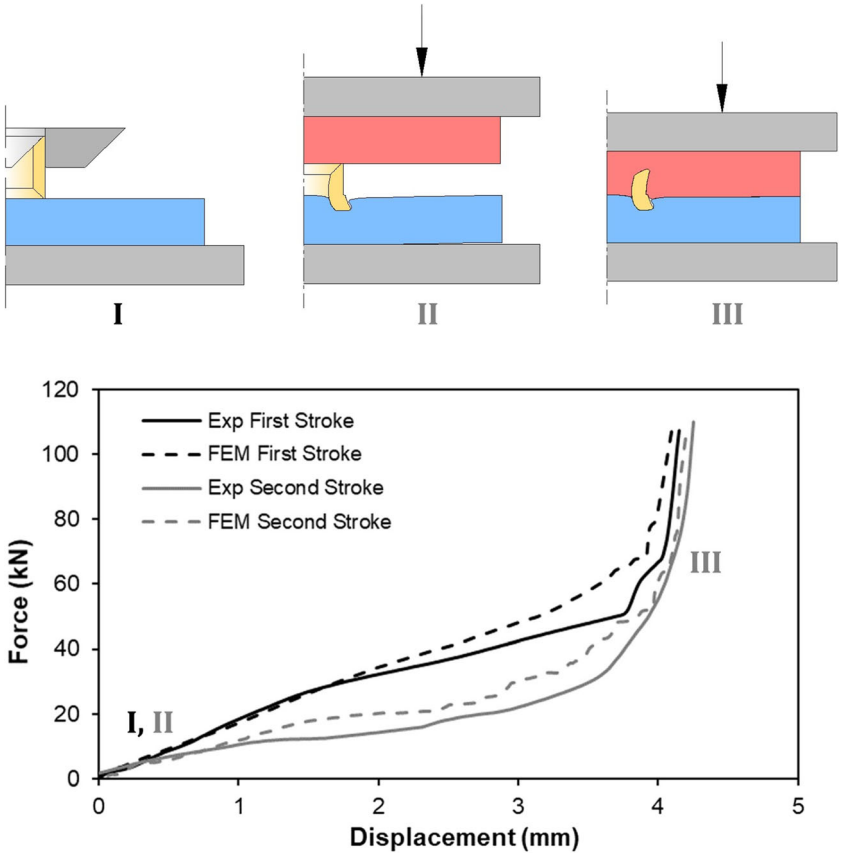


**Fig. 9** Experimental and finite element predicted evolution of the riveting force with displacement for the double-stroke double-sided self-pierce riveting of AA5754-H111 aluminum and PVC sheets with AISI 304 stainless-steel rivets ($\alpha_{alu} = 45°$, $\alpha_{pvc} = 45°$)

steel rivets by peeling, no differences in performance are expected to be found between the new AA5754-H111-PVC joints and the earlier tested monolithic PVC joints [11].

Because of the abovementioned reasons, the performance of the joints obtained by means of the new proposed two-stroke DSSPR process was solely tested in shear (refer to the testing schematic included in Fig. 10). The force vs. displacement evolution for the test case ($\alpha_{alu} = 45°$, $\alpha_{pvc} = 45°$) of Fig. 8c is compared against those previously obtained by the authors for conventional (single-stroke) DSSPR of monolithic AA5754-H111 aluminum and PVC joints.

As seen in Fig. 10, the maximum shear destructive force for detaching the AA5754-H111-PVC joints is in-between the values obtained for separating the monolithic joints made from aluminum or PVC sheets. The reason for the maximum shear destructive force of the AA5754-H111-PVC joints being greater than that of monolithic PVC joints is attributed to a change in the detaching mechanism. In fact, as seen in the

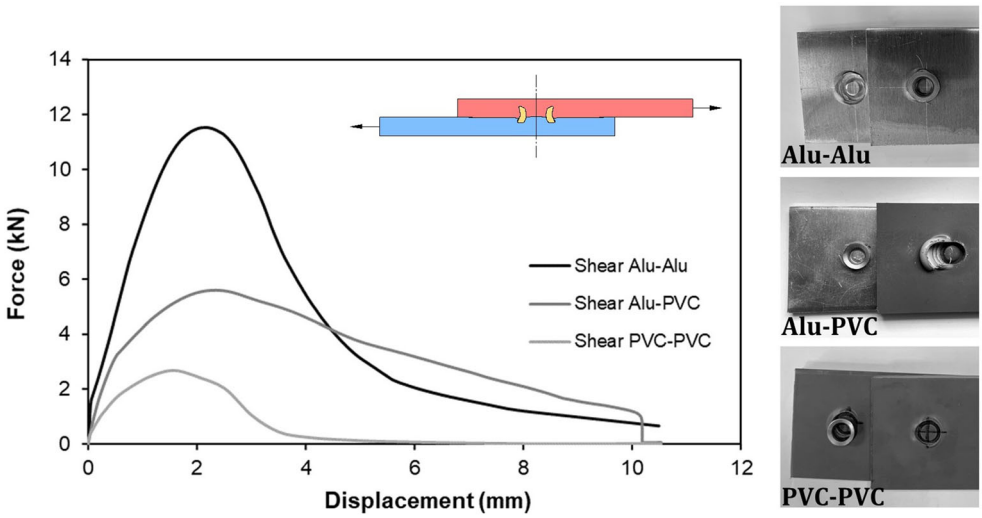


**Fig. 10** Experimental evolution of the destructive shear force with displacement for the AA5754-H111-PVC joints ($\alpha_{alu} = 45°$, $\alpha_{pvc} = 45°$) produced by two-stroke double-sided self-pierce riveting. Results for the monolithic AA5754-H111 and PVC joints are provided for reference purposes. Photographs of the shear test specimens after separation are also included

rightmost photographs of Fig. 10, the detachment of the joints made from dissimilar materials with very different strengths involves displacement of the sheet material with lower mechanical strength (e.g., PVC) ahead of the rivet with formation of ridges alongside the groove, whereas the detachment of monolithic PVC joints occurs by disengagement after distortion (no ridges are observed).

## 4 Conclusions

Two-stroke double-sided self-pierce riveting can join overlapped sheets made from dissimilar materials with very different strengths. Experimental and numerical results performed with AA5754-H111 aluminum and PVC sheets showed that good mechanical interlockings with undercut values in the range of 0.9 mm and totally hidden inside the two sheets can be obtained. Slight protrusions above the PVC sheet surfaces that are formed during unloading are caused by the low elastic modulus of PVC and are considerably smaller than those obtained in alternative joining by forming processes. Results also showed that best results are obtained for tubular rivets with chamfered angles in the range of 30 to 45° and that performances in shear destructive testing are ranked in-between those of monolithic aluminum and PVC joints.

Extension of the conventional single-stroke double-sided self-pierce riveting to the connection of overlapped sheets made from dissimilar materials with very different strengths are feasible if the tubular rivets are prepared with different chamfered angles (e.g., 30 and 60°) at their ends. However, the advantage of joining dissimilar sheets in a single-stroke comes with the price of the resulting cross-sections being highly asymmetric due to greater or lesser penetration of the rivets into the sheets.

**Acknowledgments** The authors would like to thank the support provided by Fundação para a Ciência e a Tecnologia of Portugal and IDMEC under LAETA-UIDB/50022/2020.

**Availability of data and material** The authors confirm that the data and material supporting the findings of this work are available within the article.

**Author contribution** Experimentation, Luis M. Alves, Rafael M. Afonso, Patric T. Pereira; numerical modeling, Luis M. Alves, Rafael M. Afonso, Patric T. Pereira, Paulo A.F. Martins; writing-original draft preparation, Paulo A.F. Martins; writing-review and editing, Luis M. Alves, Rafael M. Afonso, Paulo A.F. Martins; coordination, Paulo A.F. Martins.

**Funding** This work was supported by Fundação para a Ciência e a Tecnologia of Portugal and IDMEC under LAETA-UIDB/50022/2020.

## Declarations

**Ethics approval** The article follows the guidelines of the Committee on Publication Ethics (COPE) and involves no studies on human or animal subjects.

**Consent to participate** Not applicable. The article involves no studies on humans.

**Consent for publication** Not applicable. The article involves no studies on humans.

**Competing interests** The authors declare no competing interests.

## References

1. Meschut G, Janzen V, Olfermann T (2014) Innovative and highly productive joining technologies for multi-material lightweight car body structures. J Mater Eng Perform 25:1515–1523
2. Bouchard PO, Laurent T, Tollier L (2008) Numerical modeling of self-pierce riveting—from riveting process modeling down to structural analysis. J Mater Process Technol 202:290–300
3. He X, Baoying X, Kai Z, Gu F, Ball AD (2013) Numerical and experimental investigations of self-piercing riveting. Int J Adv Manuf Technol 69:1–4
4. Porcaro R, Hanssen AG, Langseth M, Aalberg A (2006) The behaviour of a self-piercing riveted connection under quasi-static loading conditions. Int J Solids Struct 43:5110–5131
5. He X, Pearson I, Young K (2008) Self-pierce riveting for sheet materials: state-of-the-art. J Mater Process Technol 199:27–36
6. Li D, Chrysanthou A, Patel I, Williams G (2017) Self-piercing riveting - a review. Int J Adv Manuf Technol 92:1777–1824
7. Kato K, Okamoto M, Yasuhara T (2001) Method of joining sheets by using new type of rivets. J Mater Process Technol 111:198–203
8. Huang Z, Xue S, Lai J, Xia L, Zhan J (2014) Self-piercing riveting with inner flange pipe rivet. Proced Eng 81:2042–2047
9. Huang Z, Yao Q, Lai J, Zhao J, Jiang Z (2017) Developing a self-piercing riveting with flange pipe rivet joining aluminum sheets. Int J Adv Manuf Technol 91:2315–2328
10. Alves LM, Afonso RM, Martins PAF (2020) Double-sided self-pierce riveting. Int J Adv Manuf Technol 108:1541–1549
11. Alves LM, Afonso RM, Martins PAF (2021) Double-sided self-pierce riveting of polymer sheets. J Adv Join Proc 3:100051
12. Nielsen CV, Zhang W, Alves LM, Bay N, Martins PAF (2013) Coupled finite element flow formulation. In: Davim JP (ed) Modelling of thermo-electro-mechanical manufacturing processes with applications in metal forming and resistance welding. Springer, New York. https://doi.org/10.1007/978-1-4471-4643-8_3
13. Nielsen CV, Martins PAF (2021) Finite element simulation: a user's perspective. In: Metal forming: formability, simulation and tool design. Academic Press, London. https://doi.org/10.1016/B978-0-323-85255-5.00011-X